| | | | |
|---|---|---|---|
| **Project acronym:** | **GeoSmart** | | |
| **Project title:** | Technologies for geothermal to enhance competitiveness in smart and flexible operation | | |
| **Activity:** | LC-SC3-RES-12-2018 | | |
| **Call:** | H2020-LC-SC3-2018-RES-SingleStage | | |
| **Funding Scheme:** | IA | Grant Agreement No | 818576 |
| WP 5 | GeoSmart Simulator and Decision Support System | | |

# D5.1 –Flow assurance simulator implementation of new geofluid models

| | | |
|---|---|---|
| **Due date:** | 31/05/2021 (M24) | |
| **Actual Submission Date:** | 08.11.2021 | |
| **Lead Beneficiary:** | FPS | |
| **Main authors/contributors:** | Per Kjellgren (FPS), Tao Peng (FPS), Hanrui Yu (FPS), Carl Birger Jenssen (FPS) | |
| **Dissemination Level[1]:** | PU | |
| **Nature:** | REPORT | |
| **Status of this version:** | | **Draft under Development** |
| | | **For Review by Coordinator** |
| | X | **Submitted** |
| **Version:** | 1 | |
| **Abstract** | This deliverable reports on the Geothermal Flow Assurance Simulator | |

## REVISION HISTORY

| Version | Date | Main Authors/Contributors | Description of changes |
|---|---|---|---|
| V1 | 05.11.2020 | FPS | First version |
| | | | |
| | | | |

This project has received funding from the *European Union's Horizon 2020 research and innovation programme* under grant agreement No 818576

[1] Dissemination level security:
**PU** – Public (e.g. on website, for publication etc.) / **PP** – Restricted to other programme participants (incl. Commission services) / **RE** – Restricted to a group specified by the consortium (incl. Commission services) / **CO** – confidential, only for members of the consortium (incl. Commission services)

*This project has received funding from the European Union's Horizon 2020 program Grant Agreement No 818576. This publication reflects the views only of the author(s), and the Commission cannot be held responsible for any use which may be made of the information contained therein.*

**CONTENTS**

# SUMMARY

A new software specialized for flow assurance simulations of geothermal installations is under development by partner FPS. The software combines fluid dynamics, thermodynamics, geochemistry, heat transfer, structural dynamics, and aims to enable simulation of most situations that arise in design and operation of geothermal installations: powerplants, wells, transport pipes, and drilling. The main objective of the work presented in this report is to further the development of this flow assurance software, with special focus on the User Interface (UI) (both graphical & text) and also addition of a reaction-advection-diffusion equation (RADE) implementation combined with the silica polymerization reaction rate model developed by partner UoI in the GeoSmart D4.1 report [1].

The report starts with a section describing all main features of the software to provide a reference for work later in this report as well as other WP5 reports. Thereafter comes a section on the User Interface, with sample screenshots of GUI, text files, and help documentation. Then a section on the development and implementation of the RADE and reaction rate model, followed by sections with simulation examples and conclusions. This report forms the basis for the work that will be performed later in WP5, with development of new device models in Task 5.2, and simulations of the Insheim and Kizildere II plants in Task 5.3 and Task 5.4.

# OBJECTIVES MET

The work described in this report contributes to the objectives of Work Package 5:

- Develop the GeoSmart system simulator suite which combines flow assurance simulator, knowledge based engineering, and decision support systems, to provide robust options for future design capability across diverse European geothermal sites, investment decision making and policy analysis.

And in particular:

- Development of a GeoSmart system simulator software
- Development of a powerful User Interface
- Development of reaction-advection-diffusion solver to enable simulation of reaction kinetics
- Implementation of silica reaction rate model developed by UoI in GeoSmart D4.1

# 1. INTRODUCTION

To enable detailed and reliable planning for exploration, design, and operation of geothermal energy facilities it is necessary to have good understanding of the operating conditions in the different parts of the piping system. To properly simulate the complex governing phenomenon involved, the simulator needs to combine thermodynamics, fluid dynamics, and geochemistry. This kind of modelling is called flow assurance and originates from the oil and gas industry, especially for offshore fields where multiphase flow need to be operated within the correct parameters to avoid or limit solid deposits such as hydrates, scale, wax, unwanted flow regimes such as excessive slugging, and operational procedures such as start-up, shut in, injection of inhibitors, etc. The term flow assurance was first used by Petrobras (Garantia do Escoamento), meaning literally "guarantee of flow". Flow assurance modelling is a relatively new area and is rapidly becoming widely used in the oil & gas industry where it is considered to be one of the most important key technologies for efficient, economical and safe oil & gas production [2].

Existing commercial software for multiphase flow simulations within oil & gas, e.g. OLGA and LedaFlow, can in principle be used also for geothermal applications. However, they are not tuned for this regarding robustness and speed, and in addition lack support for appropriate geochemistry modules. For geothermal flow assurance, though there exists software for geochemistry, reservoir, and coupled wellbore-reservoir simulations, these typically have targeted application areas, and therefore offer relatively limited features, making it difficult to find software that can simulate the full range of pipe networks, wells, devices, and operating conditions that appears in geothermal power plants. Moreover, flow assurance governing equations, especially in the case of pipe networks and rapidly closing/opening valves or phase changes, are notoriously ill-conditioned and difficult to solve. Therefore, approaches based on general software such as Comsol or Modelica are typically computationally too slow and use more generic and less complex algorithms and solvers, making it difficult to achieve adequate robustness for simulation of large flow assurance systems. To remedy this, FPS has started developing a dynamic (time-dependent) two-phase pipe network flow assurance simulator tailor-made for geothermal applications. The development of this software, Flowphys1D, is a major, multi-year undertaking that in addition to the GeoSmart project also is partly financed by several other projects (H2020: SmartRec [3], GeoCoat [4], GeoPro [5], GeoDrill [6]; Eurostars: ProCase [7]; and NRC: FORSTERK FPS Simulator [8]). It should therefore be noted that some parts of the presentation in this report, especially in Section 2, have also appeared in other reports.

In the work behind this report, the focus has been:

a) GUI development: the GUI has features such as modelling the piping systems and devices (valves, pumps, heat exchangers, etc.); providing input to parameters for pipes and devices; mesh generation to create the computational FEM mesh; providing input to solver parameters. The GUI can be used both through its menu system as well as in batch mode. This GUI development is a large task and part of the development is also taking place in the GeoPro and GeoDrill projects. However, GeoSmart is the main project regarding the GUI development; this is because a powerful GUI with clear system modelling and meshing is necessary in order to simulate the large-scale cases in Task 5.3 and Task 5.4.
b) RADE: To enable simulation and tracking of species, a Finite Element Method (FEM) solver for the Reaction-Advection-Diffusion Equation (RADE) has been developed and implemented into the Flow Assurance software. To accommodate this, the overall Flow Assurance solver has been split in to three fractional steps such that different physics can be iterated separately.
c) Reaction kinetics: Scaling occurs because of changes in pH or temperature, which lead to supersaturation of dissolved minerals or salts, causing precipitation. For geothermal powerplants, the most common scales are silica ($SiO_2$) and calcite ($CaCO_3$). Scaling is a major problem for many geothermal powerplants, making it necessary to have good understanding of operating environment (pressure, pH, temperature) as well as operational procedures (e.g. inhibitor injection). To facilitate such simulations, the silica polymerization reaction kinetics model developed by UoI in GeoSmart D4.1 [1] has been implemented into the flow assurance simulator.

Several example calculations for both single pipes and pipe networks are shown in Section 5.

# 2. GEOTHERMAL FLOW ASSURANCE SIMULATOR

## 2.1 Fundamentals

A steady-state as well as dynamic (time-dependent) two-phase pipe network geothermal flow assurance simulator software has been developed by FPS. It is based on conservation equations for mass, momentum, energy, and mass flux of each species. The numerical discretization is based on a finite element approach in space and an implicit time discretization with non-linear Newton-Raphson equilibrium iterations within each timestep. The software has many features in different domains, some of them briefly explained in this section.

**Single phase friction factor:**

Calculation of the friction factor can have a large impact on the results and is a topic which has attracted a significant amount of research for many decades, as evidenced by for example review papers such as [9]. For laminar flows, we use the Hagen-Poissueille equation, while for turbulent flows we have implemented two different methods: the iterative Colebrook-White equation and the non-iterative approximation provided by Haaland. A three-regime approach [10] has been implemented to handle laminar, transitional, and turbulent regimes, wherein the transitional regime is a weighted combination of the laminar and turbulent friction factors. To summarise, the single-phase Darcy-Weisbach flow friction factor in circular pipes is calculated as follows:

$$f = f_L = \frac{64}{Re} \qquad Re < 2000\ (laminar\ flow) \tag{2.1}$$

$$f = f_t = \left\{-1.8 log_{10}\left[\frac{6.9}{Re} + \left(\frac{\varepsilon}{3.7D}\right)^{1.11}\right]\right\}^{-2}, Re > 4000\ (fully\ turbulent\ flow) \tag{2.2}$$

$$f = y f_t + (1-y) f_L,\ \ y = \frac{Re}{2000} - 1\ ,\ \ 2000 < Re < 4000\ (transitional\ flow) \tag{2.3}$$

where $\varepsilon$ is the pipe wall roughness, D is the pipe diameter, and $\varepsilon$ /D is the relative roughness. Using these, examples of pressure drop for laminar and turbulent flows in horizontal pipes with different roughness are shown in Figure 2.1.

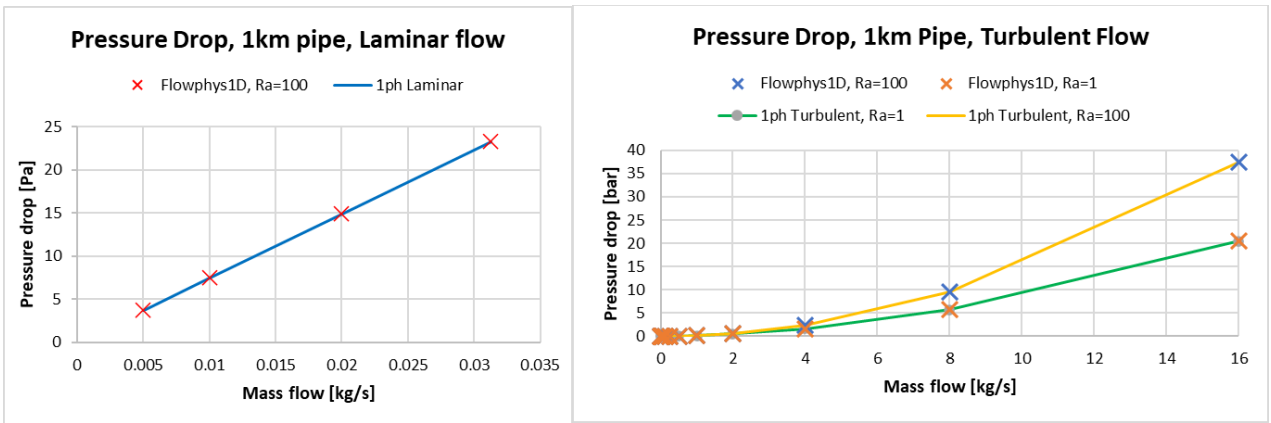


**Figure 2.1:** Pressure drop comparisons between Flowphys1D and analytic expressions for single-phase laminar- and turbulent flows [11]

**Two-phase flows models:**

Two different two-phase flow models have been implemented: a homogeneous flow model and a drift flux model. In the homogeneous model, the two phases are combined into one pseudo single-phase fluid with an average mixture velocity and average mixture fluid properties. This model assumes that there is no slip between the phases, i.e. they have the same velocities, and that the pressure and temperature are the same for both phases. This model works best for flows where the phases are well-mixed, such as for example dispersed bubble

flow. However, for cases such as for example stratified or annular flows, it may be too inaccurate due to different phase velocities. This can be improved by taking into account for different phase velocities with a drift flux model, wherein a slip velocity between the phases is introduced. There are many different versions of drift flux models. In the current Flowphys1D implementation, the model by Fabre and Line [12] is used.

**Geofluid options**

Several different options have been implemented into the FlowPhys Flow Assurance Simulator to calculate fluid properties and the dependence on temperature, pressure, and chemical composition:

- Constant properties
- Relations for properties of pure water and steam
- PVT (Pressure-Volume-Temperature) tables
- PhreeqcRM for aqueous geochemical calculations

Of these, the most powerful option is PhreeqcRM, an open-source subroutine library for aqueous geochemical calculations developed by USGS [13]. While PhreeqcRM is the most accurate method, it is also rather time consuming and prone to numerical instabilities. To improve speed and stability, we have therefore also implemented the option of using PVT tables, i.e. tables that relate pressure, specific volume, and temperature for a given fluid. Here the term is used in a slightly more general way, meaning a tabulated equation of state, and also derived properties such as viscosity, specific heat, thermal conductivity, and compressibility. The PVT tables can be generated with a FlowPhys-PhreeqcRM PVT tool, wherein geochemical calculations are carried out for a range of pressure and temperature values, or with other external geochemical calculation software. Examples of PVT tables for a liquid and a gas generated by the Flowphys1D-PhreeqcRM tool are shown in Figure 2.2. The main weakness with the PVT table approach is the underlying assumption that the fluid composition remains constant throughout the whole flow assurance simulation. For cases where this assumption is invalid, the coupled Flowphys1D-PhreeqcRM approach must be used. One such example is shown in Figure 2.3, where solubility of $CO_2$ in brine varies with pressure and temperature.

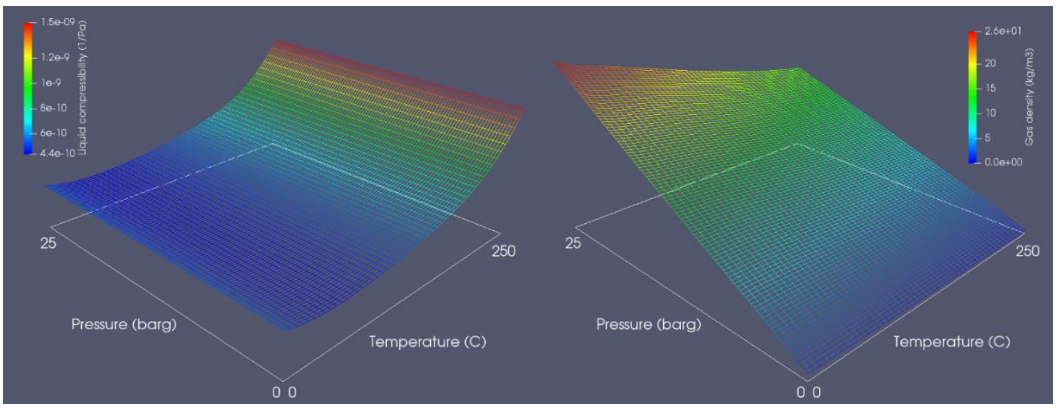


**Figure 2.2:** PVT table created by Flowphys1D-PhreeqcRM tool [14]: a) Gas density; b) Liquid compressibility

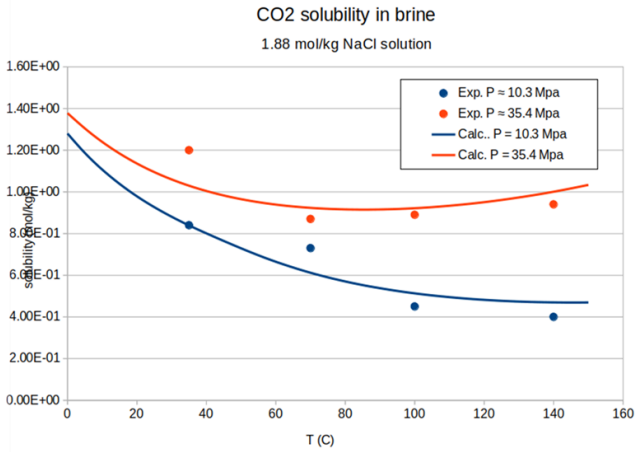

**Figure 2.3:** Solubility of $CO_2$ in brine [11]. Solid line: Flowphys1D-PhreeqcRM; Circle markers: Experiments

**Non-Newtonian fluids**

While a Newtonian fluid model is adequate for almost all gases and many common liquids such as water, it may in some cases not be accurate enough, for example for drilling fluids. To simulate such fluids, non-Newtonian fluid models have been implemented into into the Flow Assurance simulator. The main model implemented is the Herschel-Bulkley model, which can be seen as a combination of a power law model and a Bingham plastic model. The shear rate dependent viscosity of the Herschel-Bulkley model is calculated as

$$\mu(|\dot{\gamma}|) = \begin{cases} \infty & \text{for} \quad |\tau| < \tau_0 \\ K|\dot{\gamma}|^{n-1} + \dfrac{\tau_0}{|\dot{\gamma}|} & \text{for} \quad |\tau| \geqslant \tau_0 \end{cases} \tag{1}$$

where $\tau_0$ is the critical shear stress below which the fluid behaves as an elastic solid, meaning that it does not flow, $K$ is referred to as the consistency index, and $n$ the behavior index. Notice that for $n = 1$, $K = \mu$, and $\tau_0 = 0$, the constant viscosity of a Newtonian fluid is obtained. Examples of non-Newtonian fluid flow in pipes calculated with the flow assurance simulator are shown in the figures below.

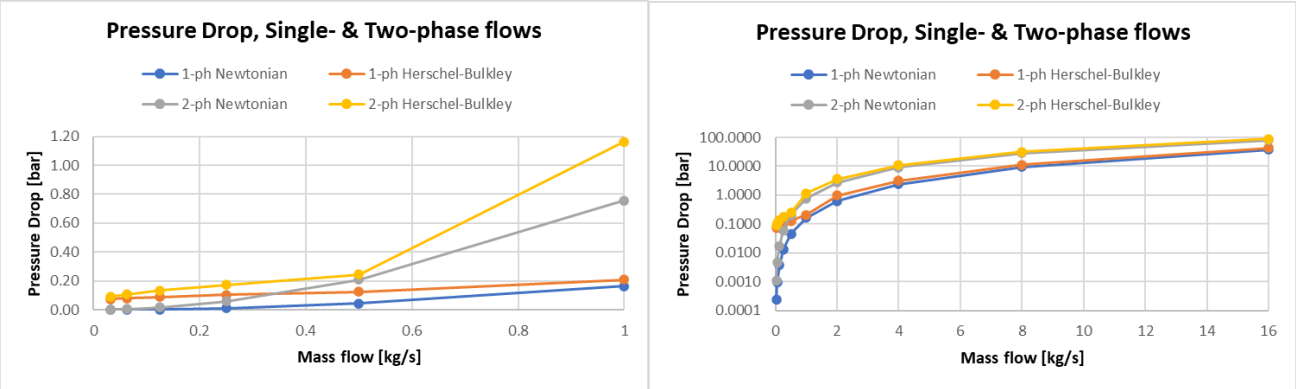


**Figure 2.4:** Pressure drop comparisons [15] for 1-phase and 2-phase flows, where the liquid part of the fluid is either Newtonian (water) or non-Newtonian (water + bentonite) modelled with the Herschel-Bulkley model.

**Corrosion, Erosion, Scaling**

Ability to simulate corrosion, erosion, and scaling are important both in the design phase as well as for optimize operational procedures (e.g. inhibitor usage) and maintenance schedules.

Corrosion:

Corrosion is often a main issue for geothermal powerplants due to aggressive geofluids. In addition to fluid composition and pipe material, other major factors are temperature, shear stresses, and pH levels. Experimental testing is difficult; flow loops can test relevant shear stresses but not able to handle neither temperatures nor the geofluids, while autoclaves or "flow reactors" can handle temperatures and geofluids but have no or almost no shear stresses. Therefore, flow assurance simulations are particurlaly important for corrosion predictions. Two different methods have been implemented for the prediction of corrosion rates: a) NORSOK model, wherein corrosion rates for carbon steel are calculated; and b) functionality for general models through a meta-modelling approach.

*NORSOK Model:* the model presented in the NORSOK standard M-506 [16] has been implemented into the Flow Assurance Simulator. This model calculates corrosion rates in hydrocarbon production and process systems made of carbon steel and where the corrosive agent is $CO_2$. This is perhaps the most commonly used model in the Oil & Gas sector. In this model model, the corrosion rate $Cr_T$ can be calculated as

$$Cr_T = K_T f_{CO2,T} f_{S,T} f_{pH,T} \quad , \tag{1}$$

where $K_T$, $f_{CO2,T}$, $f_{S,T}$, and $f_{pH,T}$, depend on temperature, CO2 fugacity, wall shear stresses, and pH level.

*Corrosion Meta-model:* To overcome limitations of the NORSOK model (e.g. geofluid composition, temperature) and provide corrosion simulations for all fluids and materials, functionality for meta-modelling has been implemented. With this, any data set (e.g. from field data, experiments, or simulations with specialized corrosion software), can be used as input to the flow assurance simulator, which then creates a meta-model that is used in the flow assurance simulations. For example, in the Geo-Coat project, we used FREECORP [17] to generate a data set for combination of $CO_2$ and $H_2S$ corrosion of mild steel, which was then used for generating a meta-model.

Erosion:
The main erosion model currently implemented into the flow assurance simulator is the DNV model [18], which is based on the assumption that erosive wear depends on the velocity and impact angle of impacting particles and furthermore that it can be estimated from the following empirical relation:

$$\dot{E_m} = \dot{m}_p K U_p^n F(\alpha) \tag{2}$$

where $\dot{E_m}$ is the erosion rate (mass eroded per unit time), $\dot{m}_p$ is the mass flow of impacting particles, $U_p$ is the particle velocity at impact, and $K$ and $n$ are experimentally determined material constants. $F(\alpha)$ is a function of the impact angle ($\alpha$). The DNV model considers smooth and straight pipes, welded joints, pipe bends, blinded Tee, reducers, flexible pipes and intrusive erosion probes. It should be noted that from a practical point of view, erosion rates in straight pipes is usually negligible.

Scaling:
Scaling is a major issue for many geothermal powerplants. To enable simulation of scaling, it is necessary to have a flow assurance simulator in order to have a good understanding of operating environment (pressure, pH, temperature, fluid composition) as well as effect of operational procedures such as management of fluid composition (dilution with non-scaling fluids, e.g. water), inhibitor injection, temperature, etc.

*Model based on Saturation Indices*: a scaling growth rate model based on the saturation index was developed in the Geo-Coat project.

*Model based on silica polymerization*: a reaction kinetics model for silica polymerization was developed by UoI in GeoSmart D4.1 [1]. This model has been implemented into the flow assurance simulator, as described in Section 4 in this report. A scaling growth rate model based on concentration of amorphous silica will be developed during 2022.

**Annulus flows**
To enable simulations during drilling operations, as well as other cases, a model for annulus flows has been implemented. Sample results with the FPS geothermal flow assurance simulator annulus model are shown in Figure 2.5. Here, the ratio Dr between the inner diameter Di and outer diameter Do is found to have a significant impact on the pressure loss: for example, with Dr=Di/Do=0.9, the pressure loss is about 14 times higher than with Dr=0.5 and about 64 times higher than a circular pipe with diameter Do (Figure 2.5a). If the annulus flow in addition is two-phase, the pressure loss is even higher (Figure 2.5b).

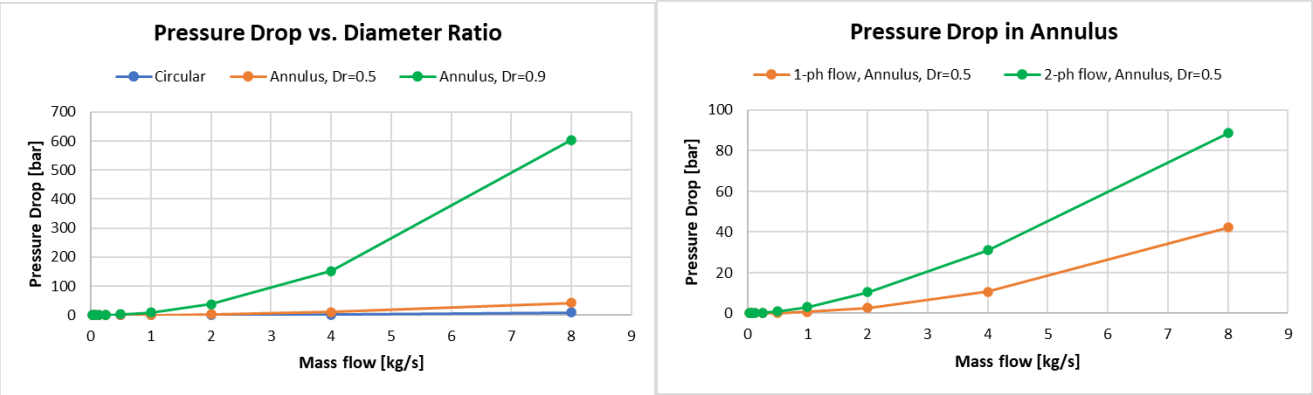


**Figure 2.5:** Pressure drop for 1-ph and 2-ph flows in annular pipes with diameter ratios Dr=(0, 0.5, 0.9) and absolute surface roughness Ra=100mm [15]

**Heat transfer to environment, annulus, or rock formation**

Heat transfer via analytic expressions for steady-state in concentric circles:

The temperature along the pipes and along an annulus is calculated by solving the energy equation. Heat flux between the surrounding and the fluid in the pipe is calculated for pipes with arbitrary many layers and materials, also insulation and rock formation is possible. Convection effects for surrounding air/water are included. Different models for heat transfer coefficients between fluid/solid interfaces have been implemented, e.g. the Dittus-Boelter model as well as the Gnielinski [19] model.

Steady-state and transient heat transfer in general geometries:

An advanced non-linear transient 3D thermo-visco-elasto-plastic mechanical FEM solver was developed in the WeldGalaxy project [20], where it was used to simulate computational welding mechanics. The solver is able to analyze general geometries and boundary conditions and use non-linear methods both for the thermal as well as the mechanical parts. For geothermal settings, this solver can conveniently be used for analyzing for example steady-state and transient heat transfer, thermal stresses, and deformations in pipes/casing/rock formation or other hot parts, as well as investigating heat-affected zones for coated parts etc. Example results from simulations of a fillet-on-corner weld are shown in Figure 2.6.

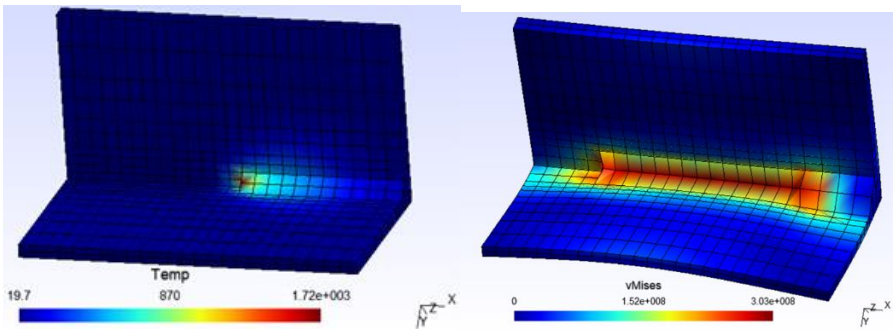


**Figure 2.6:** Examples of structural heat transfer and coupled thermo-mechanical analysis with Flowphys3D [21]. a) Heat distribution during welding. b) Residual stresses after cooling down 2 hours

**Structural Dynamics**

To enable fluid-structure interaction simulations, especially in conjunction with drilling operations, both steady-state and dynamic FEM solvers for structural analyses have been implemented. These contains a generalized 1D finite element that combines bending, tension, and torsion, with 6 DOFs (Degree-of-Freedom) at each node. An implicit Newmark method is used for time stepping. Moreover, advanced models for added mass and added damping have also been included, especially for the case of transversal vibrations of a pipe in a borehole. As an example, a comparison of a pipe vibrating inside a borehole in vacuum as well as with (quiescent) fluid is shown in Figure 7.

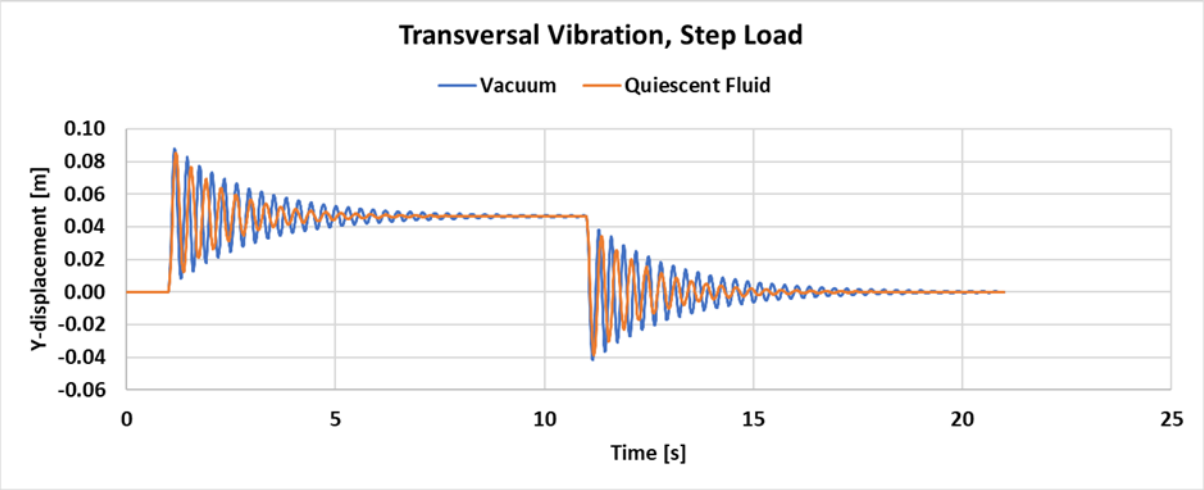


**Figure 2.7:** Time-history of free end of cantilever beam subjected to a transversal step load. Comparison of vibration in vacuum and in a quiescent fluid (=added mass and added damping included).

**Computational Fluid Dynamics (CFD) in 2D and 3D**

The software has many models and features for CFD in 2D and 3D. From a flow assurance perspective, this is important when investigating in detail, for example cavitation with complex geothermal brine (GeoPro project), droplet dynamics (GeoHex project [22]), and geothermal drilling (GeoDrill). But it is also important when developing simplified 0D or 1D models that can be used for system-wide flow assurance simulations, for example when deriving 0D/1D models for the retention tank or heat exchanger in GeoSmart WP4. Examples with detailed turbulent flow simulations using Large Eddy Simulation (LES) are shown in Figure 2.8. We often perform shape optimizations based on Design-of-Experiment (DoE), meta-modelling (typically Kriging or Artificial Neural Network), and global optimization using Genetic Algorithms. An example of original and optimized fluidic oscillators are shown in Figure 2.9. The software also includes moving boundaries and fluid structure interaction through an Arbitrary Lagrangian-Eulerian method [23]. In the Geo-Drill project, this is used to create a 0D/1D model of a geothermal drilling percussion mechanism, such that the flow assurance simulator can use it for system simulations.

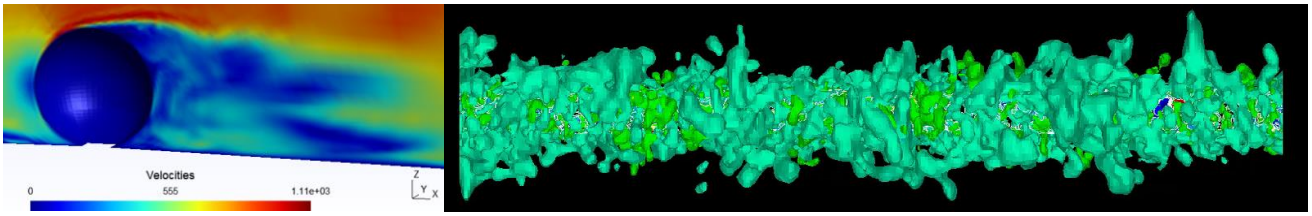


**Figure 2.8**: Large Eddy Simulation (LES) of turbulent flows. a) flow past a droplet in a geothermal heat exchanger [22]; b) turbulent boundary layer of water flowing along a circular pipe [24]

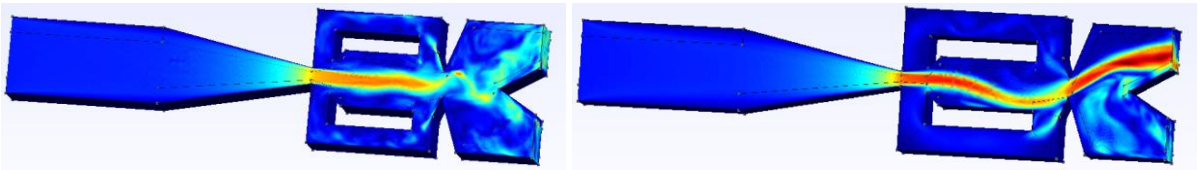

**Figure 2.9**. LES and shape optimization of a fluidic oscillator [25]. a) Original shape; b) optimized shape

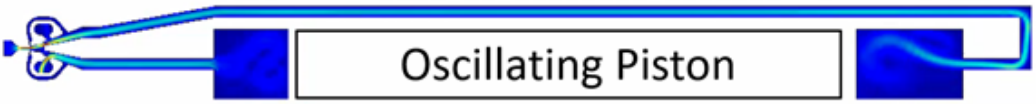


**Figure 2.10:** CFD Fluid-Structure interaction analysis of percussion mechanism [26]

## 2.2 Device models

The simulator uses a range of models for calculating mass flow, pressure, temperature in pipes and devices. Some of these models are:

- Pump
- Valve
- Turbine
- Fan
- Heat Exchanger
- Separator
- Well
- Thermal energy storage
- Annulus flow
- Leaks/injections
- Heat sinks/sources

## 2.3 Controllers

Controllers have been implemented into the software, such that process control algorithms can be simulated. An example is shown in Figure 2.3, wherein Flowphys1D used a proportional-integral-derivative (PID) controller to simulate waste-heat recovery from an intermittent heat source combined with a thermal energy storage. As explained in [27], a constant end-user power draw was possible after just 3 cycles.

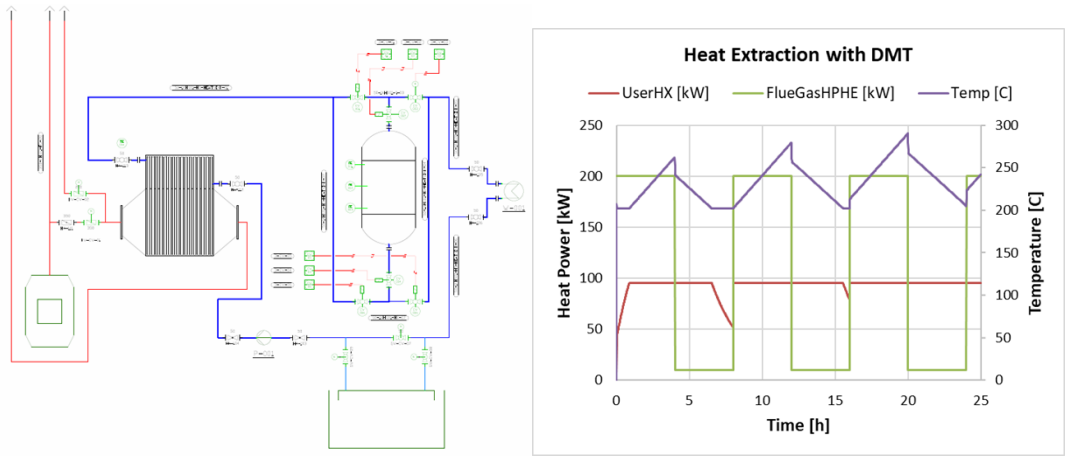


**Figure 2.3:** Example of Flowphys1D simulation using a PID controller [27]

# 3. USER INTERFACE

## 3.1 User Interface

In order to enable modelling and simulation of whole geothermal power plant installations, an extensive Graphical User Interface (GUI) is currently under development. This GUI development is a large, multi-year task and part of the development is also taking place in the GeoPro and GeoDrill projects. However, GeoSmart is the main project regarding the GUI development; this is because a powerful GUI with clear system modelling and meshing is necessary in order to build the models and simulate the large-scale cases in Task 5.3 (a part of the Insheim power plant and wells) and Task 5.4 (a part of the Kizildere 2 powerplant and wells).

The GUI includes functionality for creation of conceptual piping diagrams, modelling of geometries and pipe layouts, input of parameters for pipes (e.g. pipe wall thickness, pipe material, insulation thickness, insulation material, etc.) and devices (e.g. pumps, valves, heat exchangers, separators, etc.), input of parameters for solver, input of fluid composition, generation of the computational finite element mesh, simulation management, post-processing of results, optimisation, and more. The GUI can be used both through its menu system as well as in batch mode, and it also includes functionality for macro language with logical functions. The GUI also has help functions and direct linking to off-line and online user manuals and tutorials. It should be noted that the GUI is under development and some of the functionality is currently only partly implemented.

Some screenshots of the GUI is shown below. Figure 3.1 and Figure 3.2 show X-Z and X-Y views of a model with surface piping, devices, one production well, and one injection well. Zoom-in/out as shown in Figure 3.2 is done with the mouse wheel.

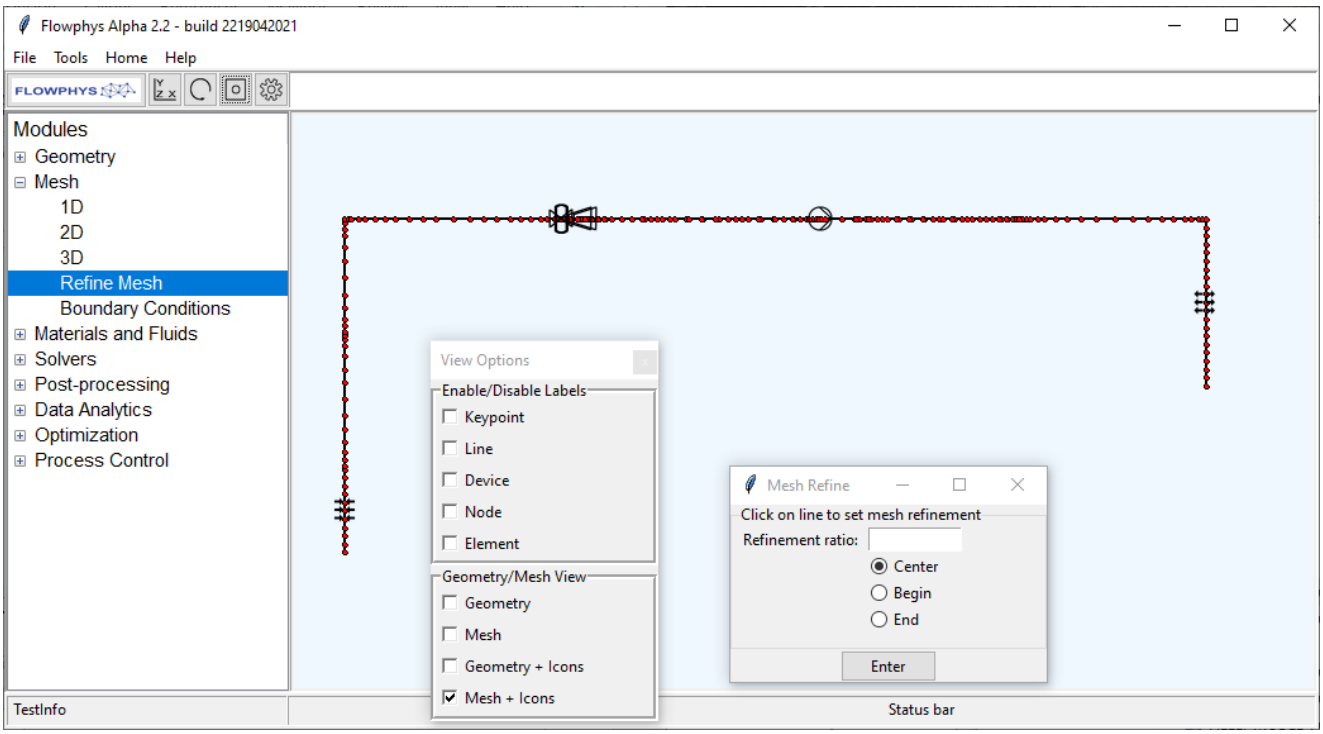


**Figure 3.1:** Example of a flow assurance model and mesh in the Flowphys1D GUI viewed in X-Z plane. Red dots represent finite element nodes; icons represent device models (e.g. production- and injection wells, pumps, valves, turbines, heat exchangers, separators, heat exchangers, etc.).

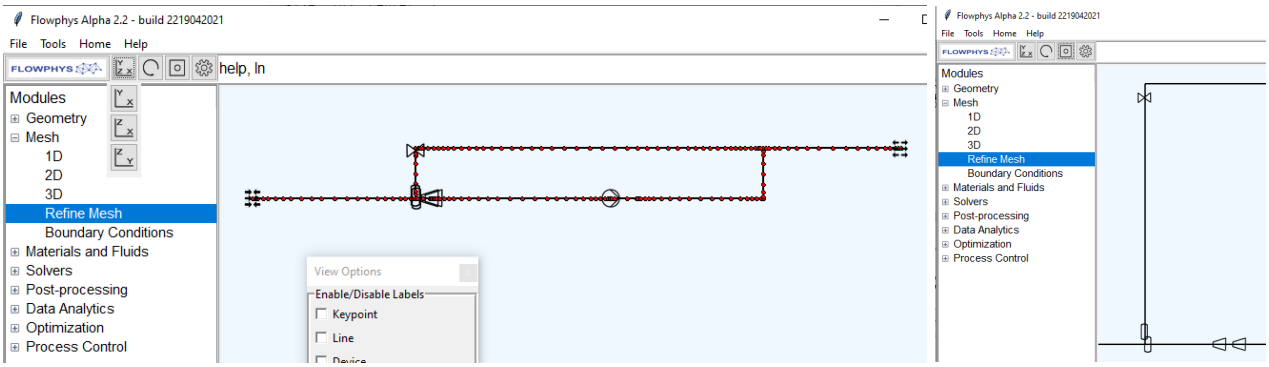


**Figure 3.2:** Same model as in Figure 3.1, but viewed in X-Y plane. a) whole model; b) zoom-in.

Every functionality that can be used via the GUI menu system, can also be used via input files. This makes it easier to build large and complex models, and to have good control and ability to document the many input parameters for different pipes, devices (e.g. pump curves, etc.), and solver settings. The input files can be used both via the GUI by a loading function, or completely in batch mode such that automated parameter scanning and parameter optimization can be carried out. There are also commands for variable definitions, looping, and conditional statements, such that the input files can also be used to create macros, and even hierarchy of macros. An example of a input file, "demo3", is shown in Figure 3.3 below, where it generates files "mesh_out", "bc.dat", "para.dat", which are subsequently used by the solver to generate the result files.

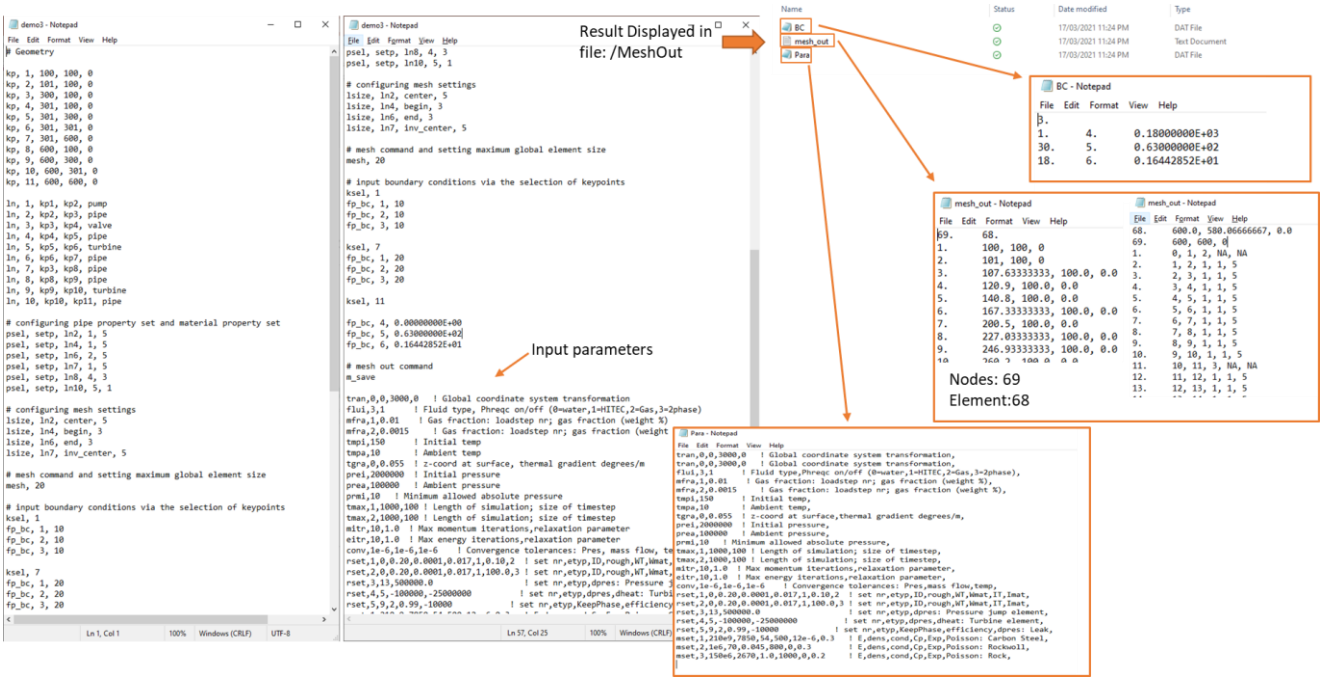


**Figure 3.3:** Screenshots of a Flowphys1D input file and some of the files it generates. The input files and macro files can be used both through the GUI menu system or in batch mode.

To help the user, the GUI has several help functions. For example, if the user put in a command in the command input box, there is a command prediction functionality to help guiding the user with the command syntax, see Figure 3.4. The user can also directly access the manual pages for the command in question by simply type "help, <command>". The manual pages can also be accessed through the GUI menu. The user manual is available both online (updated version) and offline (version at installation). An example of using the help function and a screenshot of the corresponding user manual command entry is shown in Figure 3.5.

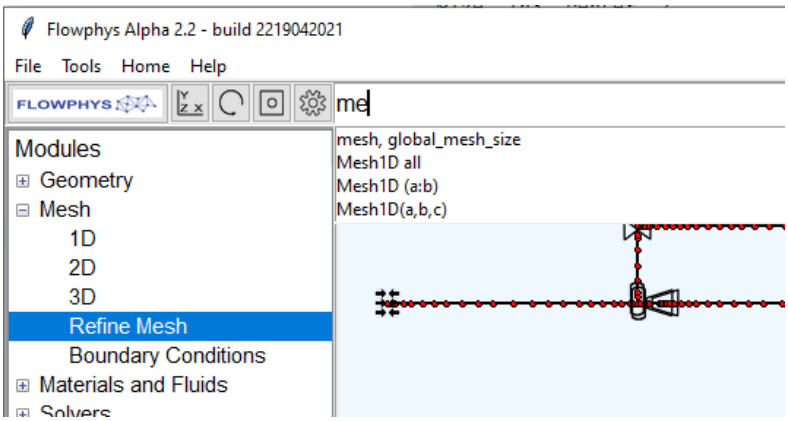


**Figure 3.4:** All commands can be accessed from the GUI menu system, or the GUI command input box, or an input file. The GUI command input box has command prediction as well as displays command arguments to aid users.

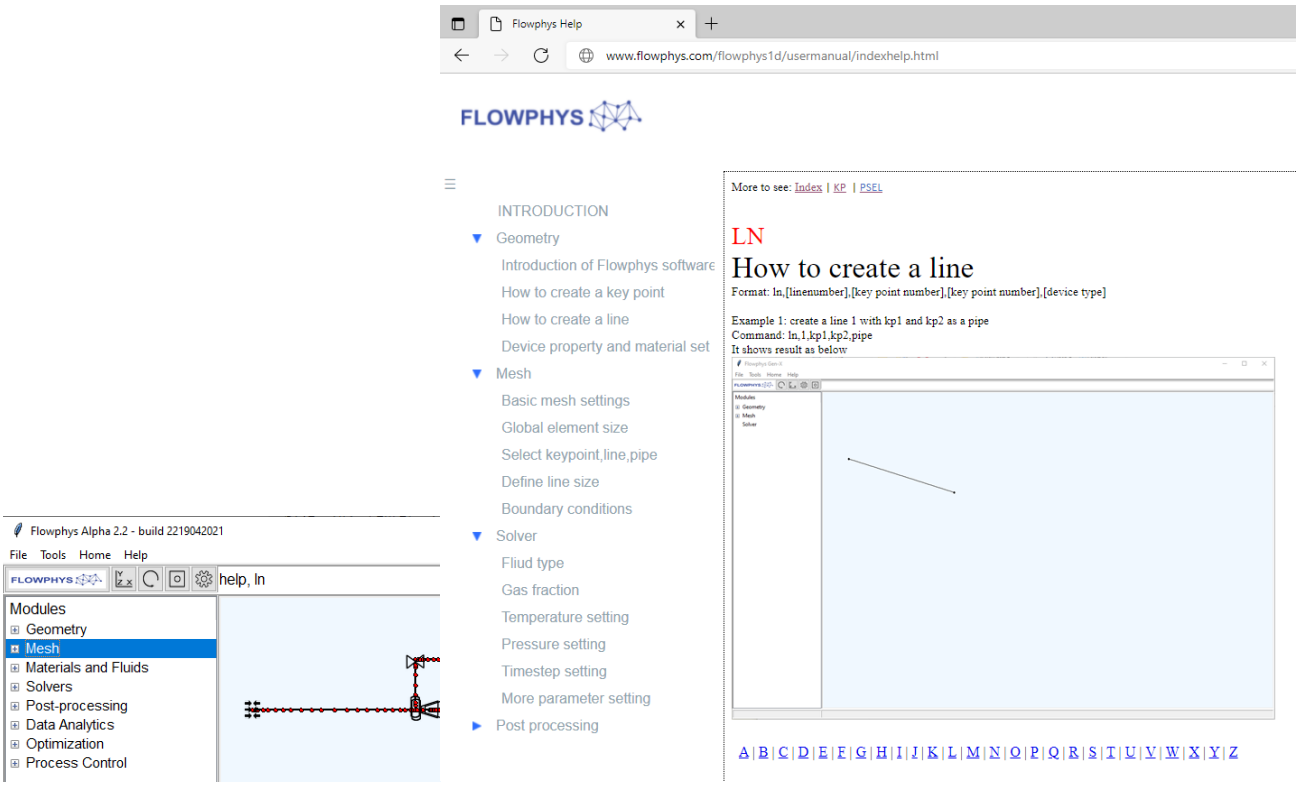


**Figure 3.5:** A powerful help system provides help for all commands. It also contains manuals and tutorials. The help system can be reached through the GUI menu system, or directly via typing "help, <command>". The help system exists both online and offline.

For building the model for simulation of wells during production/injection as well as during drilling operations, a specialized GUI module is under development, with a sample screenshot of the current prototype shown in Figure 3.6. This module will make it easier to input all the necessary information for the well casings, annuli, cementing, rock formation, as well as drill string and drilling operation.

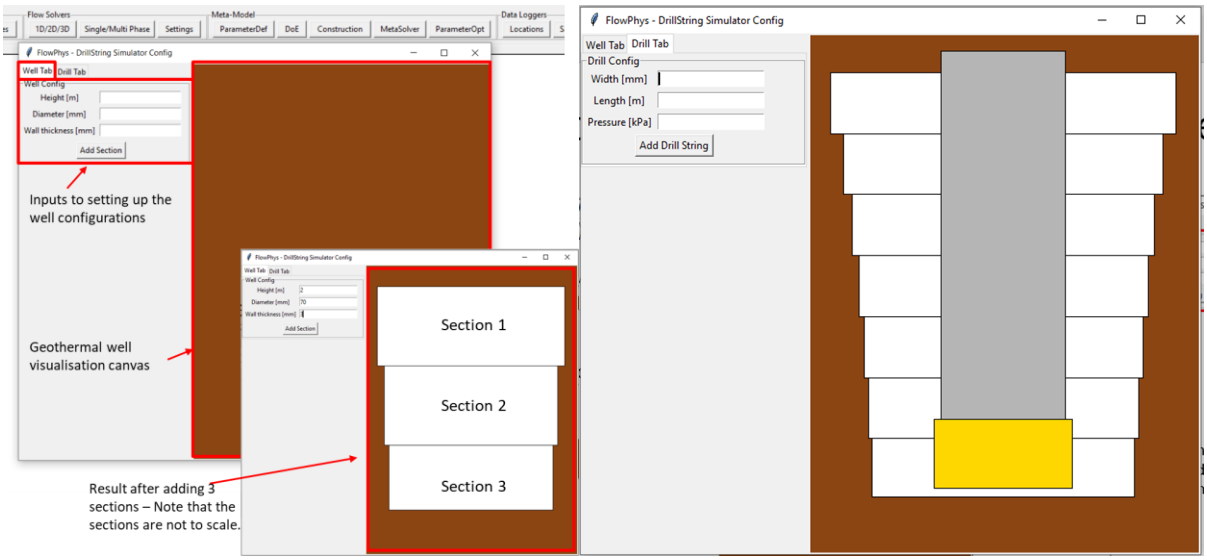


**Figure 3.6:** Flowphys1D well and drilling GUI module to simplify creation of wells, casings, annuli, cementing, drill string, and drilling operation

# 4. DEVELOPMENT OF REACTION-ADVECTION-DIFFUSION SOLVER

## 4.1 Extension to the Reaction-Advection-Diffusion problem

Scaling occurs in geothermal wells and powerplants, usually because of pressure or temperature drops. Typically, the pressure decreases cause CO2 to degas, increasing the pH, and resulting in supersaturation of dissolved minerals or salts, leading to precipitation (formation of a solid phase). Similarly, a temperature drop can also cause supersaturation and precipitation. Part of the solids will stick to the surface of the pipes and equipment, i.e. cause scaling. The most common geothermal scales are silica (SiO2) and calcite (CaCO3). Scaling is a large problem for many geothermal powerplants as it can block the pipes and equipment. Production wells and heat exchangers are typical problem areas, but perhaps the largest impact is the need to keep the pH and temperature at the injection well such as to avoid scaling to happen there. Especially, it makes it necessary to keep the reinjection temperature relatively high, often above 100 C, thereby significantly reducing the potential energy outtake from the brine. In the GeoSmart project, a system that combines a heat exchanger and a retention tank is under development, wherein the operation will be such that a large part of the solid precipitation happens in the retention tank, where it is easy to remove. With this system, it will be possible to reinject at lower temperature without risking scaling in the injection well.

In order to analyze the solids formation in the brine, it is necessary to take into account the reaction kinetics. Thus, in addition to the equations for mass, momentum, and energy conservation, we also need the convection-diffusion-reaction equation for the conservation of species,

$$\frac{\partial}{\partial t}(c) + \frac{\partial}{\partial x}(cU) = \frac{\partial}{\partial x}\left(K_L \frac{\partial c}{\partial x}\right) - R \tag{2}$$

where c is the cross-sectional mean concentration, U is the mean flow velocity, $K_L$ is the longitudinal dispersion coefficient accounting for molecular and turbulent diffusion and dispersion, and R is the reaction source/sink term. For laminar flows, the longitudinal dispersion coefficient is calculated from the Aris-Taylor dispersion,

$$K_L = \beta + \frac{U^2 r^2}{48\beta} \tag{4.2}$$

where r is the pipe radius of the pipe and $\beta$ is the diffusivity. For turbulent flows with Re>20000, the longitudinal dispersion coefficient is commonly calculated from Taylor [28] dispersion,

$$K_L = 10.1 r U^* \tag{4.3}$$

where $U^*$ is the frictional velocity,

$$U^* = U\sqrt{f/8} \tag{4.4}$$

where $f$ is the Darcy-Weisbach friction factor from Equation (2.2). Notice that Taylor's expression is based on data from high Re number experiments, Re=20000 and upwards, and is inaccurate for low Re numbers. We overcome this by creating a power law curve fit to the experimental data of Hart et al [29], see Figure 4.1 below.

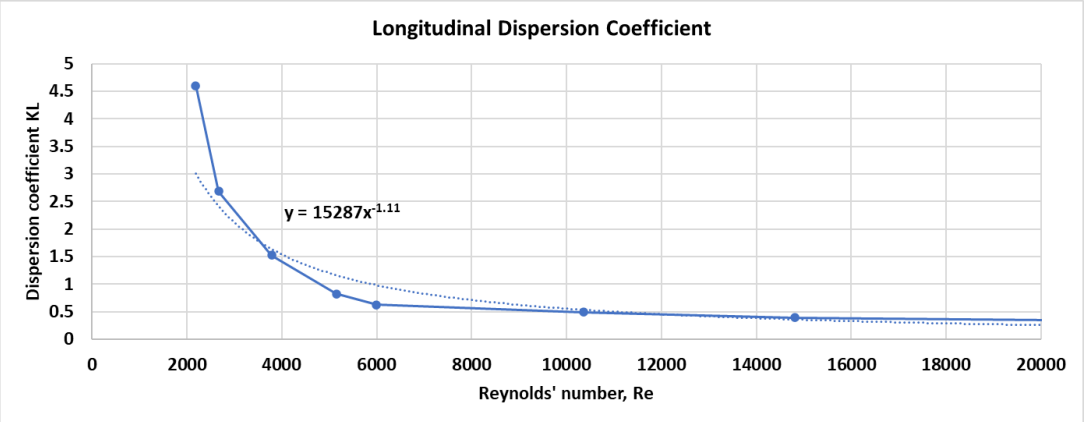


**Figure 4.1:** Longitudinal dispersion coefficient

To summarize, the longitudinal dispersion coefficient over the full span of Re-number is calculated as

$$K_L = \beta + \frac{U^2 r^2}{48\beta}, \qquad Re < 2000\ (laminar) \tag{4.5}$$

$$K_L = 2rU * 15287Re^{-1.11}, \qquad 2000 < Re < 20000\ (transitional + low\ Re\ turbulent) \tag{4.6}$$

$$K_L = 10.1rU\sqrt{f/8}, \qquad Re > 20000\ (turbulent) \tag{4.7}$$

### 4.2 Silica polymerization reaction kinetics

A new model for amorphous (AM) silica polymerization was developed in GeoSmart delivery report D4.1 [1], with the purpose to, in conjunction with flow assurance simulations, enable prediction of AM silica scaling in geothermal installations. In this model, the silica polymerization rate is

$$R = k\left(c_{SiO_{2(aq)}} - c_{SiO_{2(aq),eq}}\right)^4 \tag{4.8}$$

where $k$ is the reaction rate constant, $c_{SiO_{2(aq)}}$ is the concentration of $SiO_{2(aq)}$, and $c_{SiO_{2(aq),eq}}$ is the equilibrium concentration of $SiO_{2(aq)}$. Based on experimental data from the literature, the reaction rate constant was calculated as

$$k = Aexp(-E_a/RT)a^3_{H_4SiO_4,aq}a^{-0.75}_{H^+} \tag{4.9}$$

where A is $(3.95\pm1.16)\cdot10^6$, $E_a$ is the activation energy with value of 13.9±9.8 kJ, R is the gas constant, T is the temperature, and $a_{H_4SiO_{4(aq)}}$ and $a_{H^+}$ are the activities of aqueous $H_4SiO_{4(aq)}$ and $H^+$ species. These parameter values are valid at temperatures 20-80 C and pH between 3-10.

### 4.3 Discretization

With the addition of the Reaction-Advection-Diffusion equation, the set of governing equations is

$$\begin{cases} \dfrac{A}{a^2}\dfrac{\partial p}{\partial t}+\dfrac{\partial \dot{m}}{\partial x}=0 \\ \dfrac{\partial \dot{m}}{\partial t}+\dfrac{\partial U\dot{m}}{\partial x}+A\dfrac{\partial p}{\partial x}+\rho g A\dfrac{\partial z}{\partial x}+\dfrac{f\dot{m}|\dot{m}|}{2\rho DA}=0 \\ \dfrac{\partial}{\partial t}(\rho CTA)+\dfrac{\partial}{\partial x}(CT\dot{m})=\dfrac{\partial}{\partial x}\left(\lambda A\dfrac{\partial T}{\partial x}\right)+\phi \\ \dfrac{\partial}{\partial t}\left(c_{SiO_{2(aq)}}\right)+\dfrac{\partial}{\partial x}\left(Uc_{SiO_{2(aq)}}\right)=\dfrac{\partial}{\partial x}\left(K_L\dfrac{\partial c_{SiO_{2(aq)}}}{\partial x}\right)-k\left(c_{SiO_{2(aq)}}-c_{SiO_{2(aq),eq}}\right)^4 \end{cases} \tag{4.10}$$

where A is the cross-sectional area, a is the speed-of-sound, p is the pressure, $\dot{m}$ is the mass flow rate, U is the mean velocity, ρ is the density, g is the gravity constant, D is the pipe diameter, C is the heat capacity, T is the temperature, $\lambda$ is the heat conductivity, p is a heat source/sink, $c_{SiO_{2(aq)}}$ is the silica concentration, $K_L$ is the longitudinal dispersion coefficient, and k is the reaction rate constant.

All conservation equations in Eq. (4.10) are spatially discretized with 2-noded finite elements. For time integration, the $\theta$ -method is used:

$$\frac{p^{n+1}-p^n}{\Delta t}+\theta F(p^{n+1},t^{n+1})+(1-\theta)F(p^n,t^n) \tag{4.11}$$

Notice that setting $\theta$=0 gives the first order explicit forward Euler scheme, $\theta$=0.5 gives the implicit second order Crank-Nicolson scheme and $\theta$=1 gives the first order backward Euler scheme. As C-N is the more accurate method, it is desirable. However, with $\theta$=0.5, numerical ripples may appear, leading to inaccuracies. By setting $\theta$ slightly larger than 0.5, these numerical ripples are dampened out, and while the accuracy formally is reduced to first order, it will be close to second order accuracy as the coefficient in front of the leading error term is small. For the calculations performed in this report, $\theta$=0.51 was used.

Pipe Network Conditions

For pipe networks, extra conditions are needed at junction nodes. These can be chosen in different ways. In the FlowPhys1D code, we have chosen to conserve mass flow rate $\dot{m}$, heat flux $q$, and silica molar flux *J*. Thus, for a junction with k pipes, the following equations are fulfilled:

$$\begin{aligned} \sum \dot{m}_k &= 0 \\ \sum q_k &= 0 \\ \sum J_k &= 0 \end{aligned} \tag{4.12}$$

In addition, the pressure $p$, temperature $T$, and concentration *c* are also required to have the same values at the junction node. These requirements are illustrated in Figure 4.2 for the case of a junction node with three pipes.

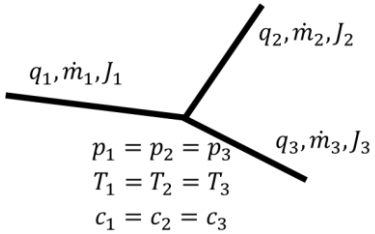


**Figure 4.2:** Conditions fulfilled at junction nodes.

### 4.4 Overall algorithm

The most accurate and correct way to solve the combined problem of fluid flow, heat transfer, and silica concentration, is to solve them all simultaneously. However, doing so would result in a complicated and large matrix, leading to slow computations. To avoid this, we are instead solving them in a sequential, staggered way. While this creates coupling errors, these errors are made small by Newton-Raphson equilibrium iterations in each timestep. Moreover, while the physics of mass and momentum conservation are strongly coupled, heat- and concentration equations are only loosely coupled with the fluid equations. This approach with de-coupling of the equations leads to faster computations. The fluid properties are calculated at the start of each timestep and kept constant during the different physics steps and the N-R iterations. The overall solution strategy and algorithm is shown in the flow chart in Figure 4.3.

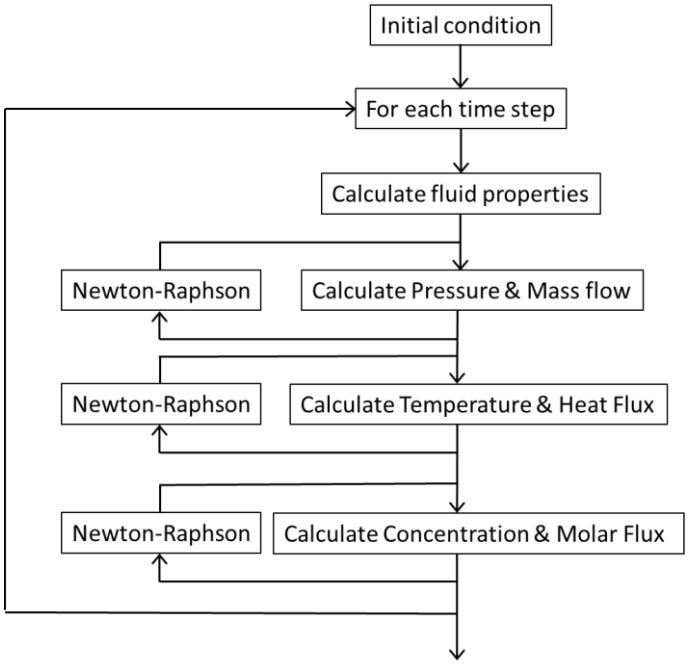


**Figure 4.3**: Flow chart of overall solution methodology

# 5. SIMULATION EXAMPLES

### 5.1 Species transport without reaction

In this example, to see the behavior of the longitudinal advection and dispersion, we assume that there is no reaction. While it would be sufficient to solver for only the advection-diffusion equation, the purpose is to validate the flow assurance software. Thus, the full set of governing equations are included,

$$\begin{cases} \dfrac{A}{a^2}\dfrac{\partial p}{\partial t} + \dfrac{\partial \dot{m}}{\partial x} = 0 \\ \dfrac{\partial \dot{m}}{\partial t} + \dfrac{\partial U\dot{m}}{\partial x} + A\dfrac{\partial p}{\partial x} + \rho g A\dfrac{\partial z}{\partial x} + \dfrac{f\dot{m}|\dot{m}|}{2\rho DA} = 0 \\ \dfrac{\partial}{\partial t}(\rho CTA) + \dfrac{\partial}{\partial x}(CT\dot{m}) = \dfrac{\partial}{\partial x}\left(\lambda A\dfrac{\partial T}{\partial x}\right) + \phi \\ \dfrac{\partial}{\partial t}(c) + \dfrac{\partial}{\partial x}(cU) = \dfrac{\partial}{\partial x}\left(K_L\dfrac{\partial c}{\partial x}\right) - R \end{cases} \tag{5.1}$$

Notice that the reaction is not included in this example, i.e. R=0. To compare the computational results with analytical results, we chose a test case with a horizontal straight pipe, constant flow velocity, and with a sudden change of concentration at the inlet. The exact solution profile can be calculated with the analytical solution [30],

$$c(x,t) = \frac{c_0}{2} erfc\left(\frac{x - Ut}{\sqrt{4K_L t}}\right) \tag{5.2}$$

where *erfc* is the complementary error function. The computations were first run with the steady-state solver to achieve a constant flow velocity in the pipe and with zero concentration. Then the concentration at the inlet was instantaneously set to 1.0 at the inlet, and the transient computation started. The computational and analytical results are shown in Figure 5.1, where profiles at two different time instants are plotted. As can be seen, the flow assurance FEM computations agree very well with the analytical solution for both t=20s and t=50s. The pipe is 100 m long and has a cross-section area of 1 $m^2$, the computational mesh consists of 100 elements, density was set to 1.0 $kg/m^3$, diffusivity was set to 1.0, bulk flow velocity in the pipe was 1.0 m/s, and the timestep size was set to 1.0 s.

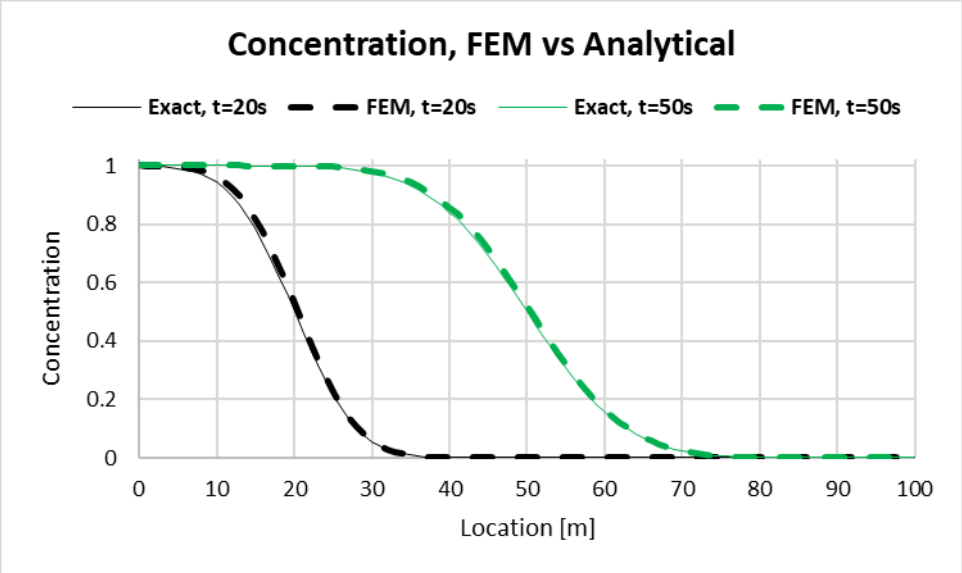


**Figure 5.1**: Comparison of exact solution and results calculated with the FEM flow assurance simulator

### 5.2 Reaction-Advection-Diffusion with constant reaction rate

Here we look at the same example as in the case above, but with reaction added to the governing equations. The governing equations are the same as in the previous example, but with R=k*concentration. The computations were performed in the same way, with first steady-state solution followed by transient solution. The same mesh and timestep sizes were used. Results are shown in the form of concentration profiles at two different timesteps. The exact analytical solution for this case is

$$c(x,t) = \frac{c_0}{2} e^{-kx} erfc\left(\frac{x - Ut}{\sqrt{4K_L t}}\right) \tag{5.3}$$

The computational and analytical results are shown in Figure 5.2 and are in very good agreement for both t=20s and t=50s.

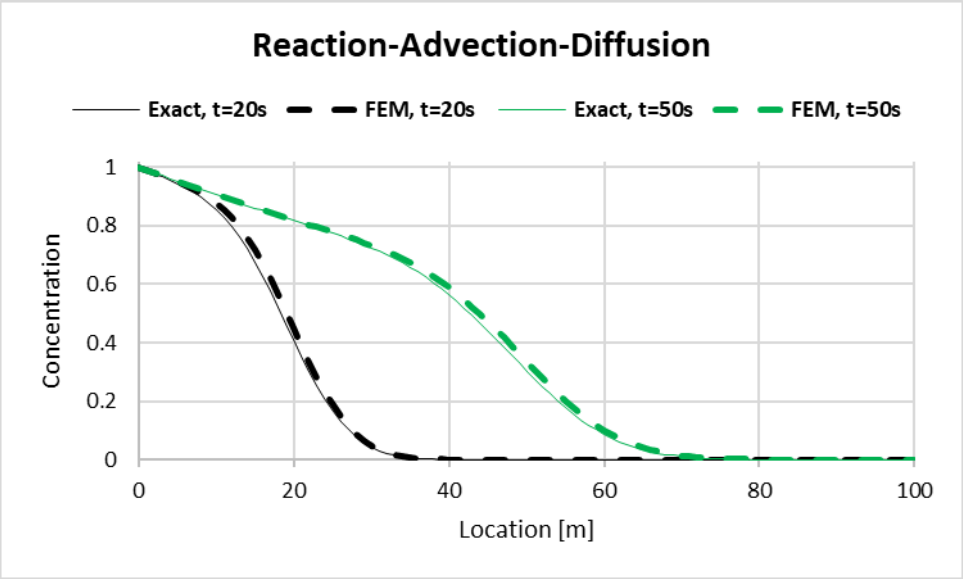


**Figure 5.2**: Comparison of exact solution and results calculated with the FEM flow assurance simulator

### 5.3 Silica reaction kinetics with new reaction rate model

In this test case, the new silica polymerization reaction rate model was used, i.e. the four equations in Eq. 4.10 were used. Because the silica polymerization is slow, the flow velocity was reduced to 0.01 m/s and the computation was run for 5000 s. The longitudinal dispersion coefficient was calculated according to Equations 4.5-4.7. The results are shown in Figure 5.3 below.

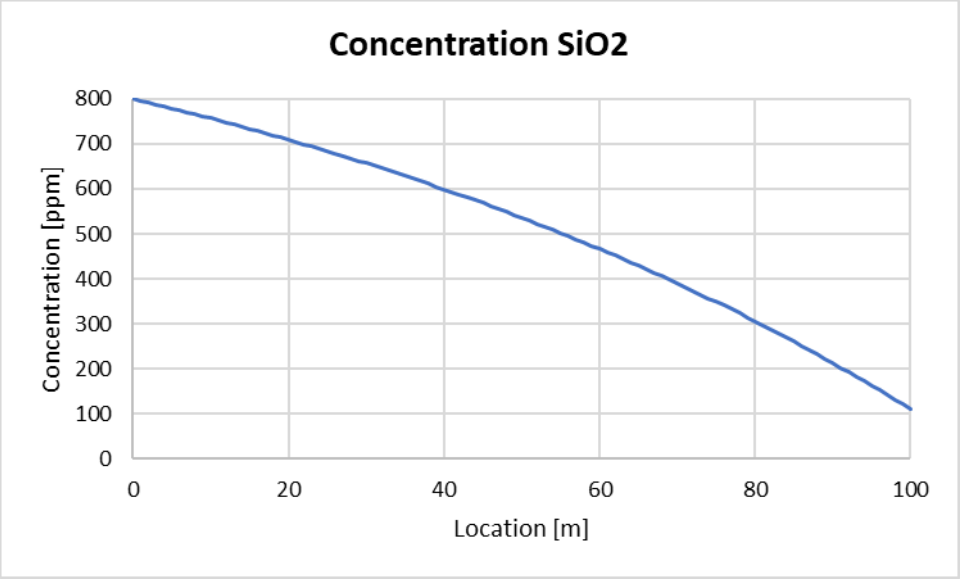


**Figure 5.3**: Silica concentration as computed with equation set Eq. 4.10, using the new silica polymerization rate model.

### 5.4 Silica reaction kinetics in a pipe network

From a numerical point of view, simulating flows in pipe networks is considerably more difficult than simulating flows in a single pipe, with the overall system often being several orders of magnitude more ill-conditioned. When also including devices, especially separators at junction nodes, or rapid transients such as closing/opening valves, or driving a "pig" through the pipe network, issues related to numerical stability and robustness can become very significant and it might be difficult to find a convergent solution.

To provide a clear, easily defined network test case, we have created the pipe network model shown in Figure 5.4, wherein the pipes are fully horizontal and no devices are included. To showcase effects of different flow

speeds, the five pipes in the middle have different diameters. The fluid composition is representative for a geothermal power plant, and Flowphys1D flow assurance simulator is using its coupling to the PhreeqcRM library to perform geochemical calculations. The boundary conditions were: mass flow=100kg/s at the inlet on the left side, and Pressure =20 bar on the right-hand side. Temperature was set to 160°C at the inlet, and 60°C at the outlet.

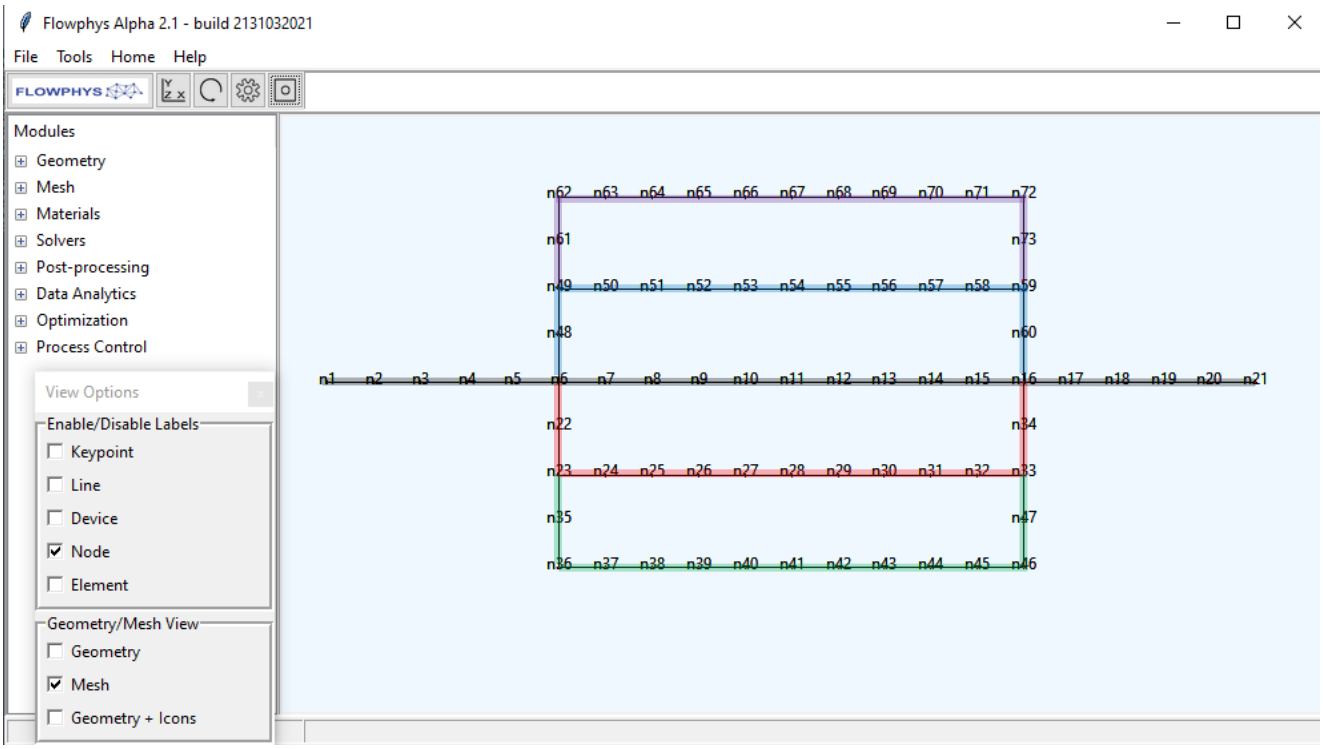


**Figure 5.4:** Mesh and color-code of pipe network case

Notice that when plotting pipe networks, we use the "length" coordinate to describe the pipe location. To simplify identification of pipes in the results plots, we have used the same colour as indicated in Figure 5.4. Simulations were performed using Flowphys1D and the results are shown in Figures 5.5-5.9. Notice that except for the silica concentration shown in Figure 5.5, all other results are identical to what has been presented before in the GeoPro project [11]. They are included in this report also for completeness, and to provide example of typical results that can be calculated with the flow assurance simulator.

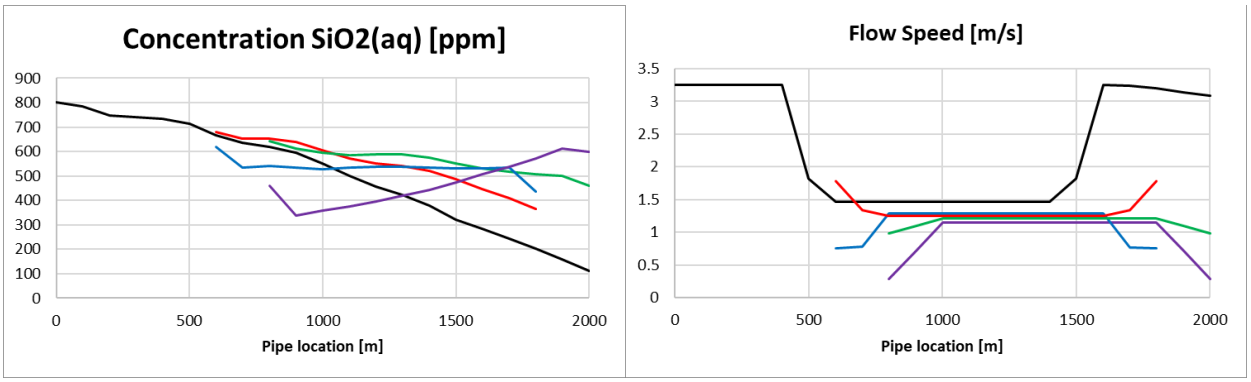


**Figure 5.5**: Silica concentration and flow speed profiles, pipe network case

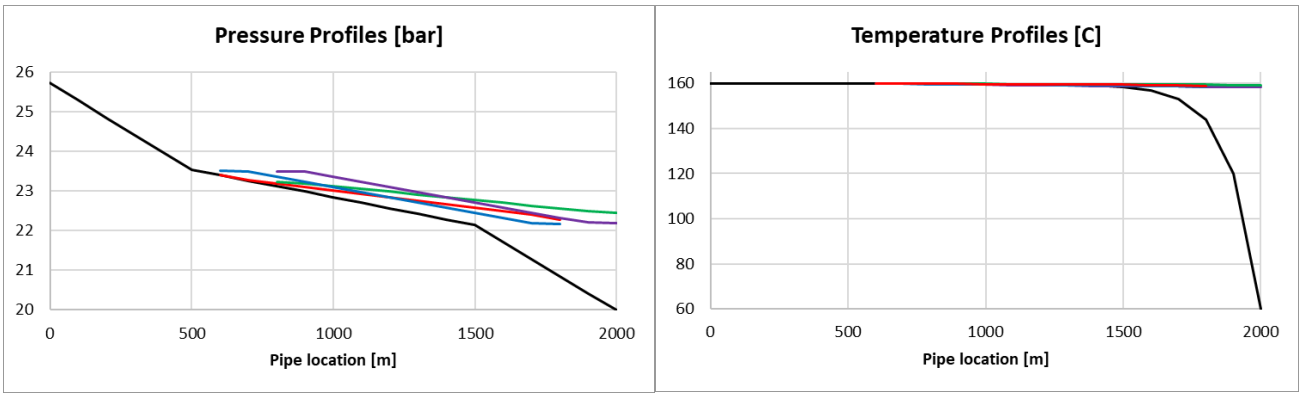


**Figure 5.6**: Pressure and temperature profiles

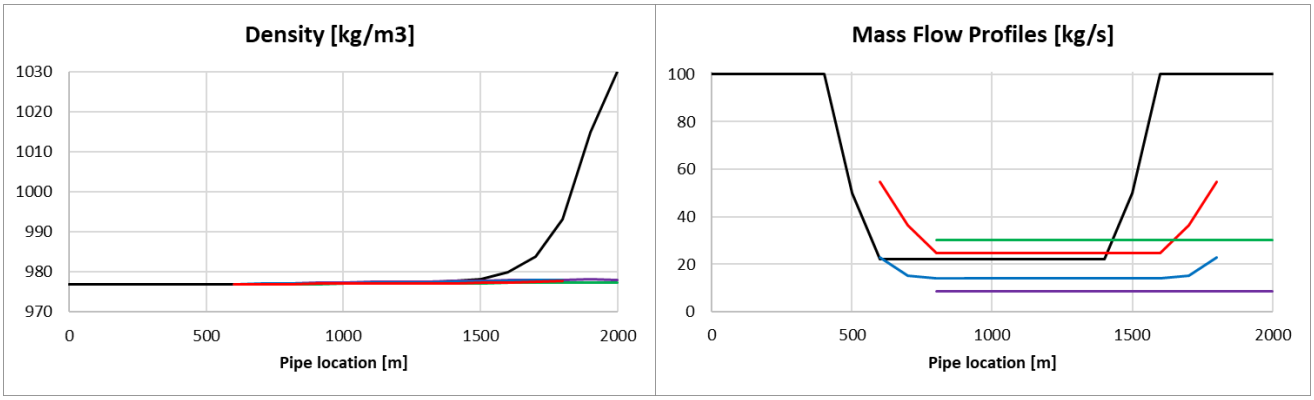


**Figure 5.7:** Density and mass flow profiles

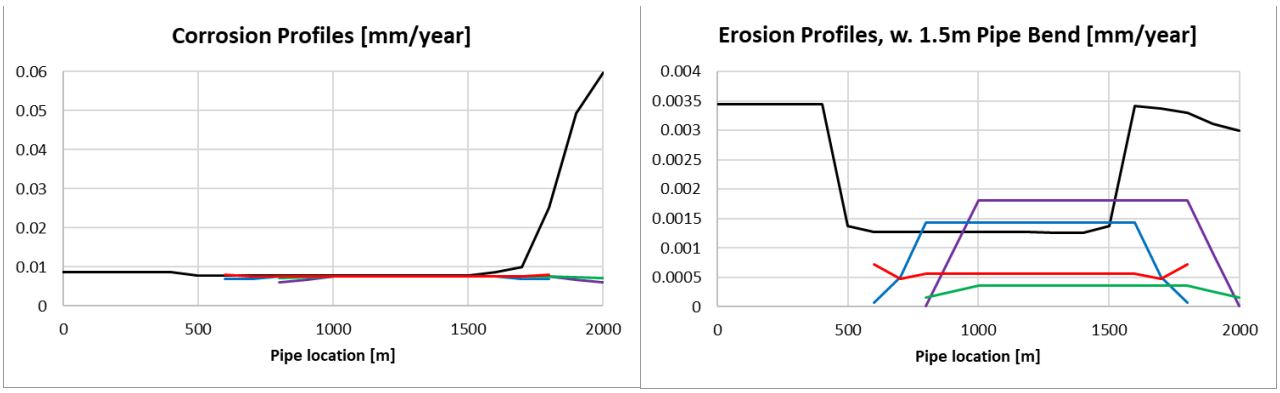


**Figure 5.8**: Corrosion and Erosion profiles. Notice: the corrosion rate is calculated with the NORSOK M-506 model [16], which is not fully valid for this case as in some locations the temperature, pH, $CO_2/H_2S$ concentrations are out-of-range. For such locations, extrapolated values of the M-506 model have been used. The erosion rate is calculated with the DNV-RP-0501 model [18], where we have focused on erosion of a pipe bend with radius 1.5m.

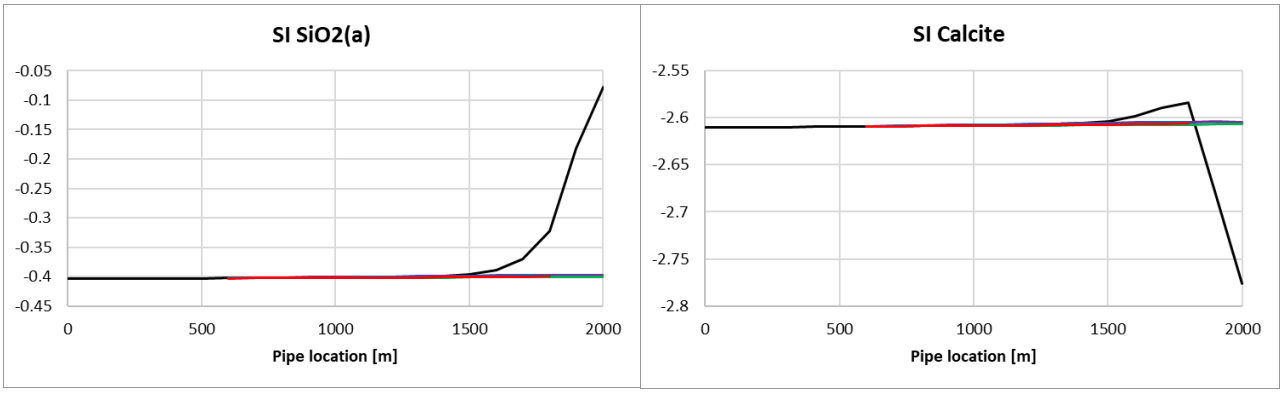


**Figure 5.9:** Saturation index profiles for amorphous silica and calcite

# 6. CONCLUSIONS

The Flowphys1D flow assurance finite element software has been extended with a reaction-advection-diffusion solver. It has been implemented as a core part of the software suite, and can therefore be used in conjunction with other features in the software, such as single- and two-phase flows, non-Newtonian fluids, geochemistry calculations through coupling with the PhreeqcRM library, heat transfer, thermodynamics, etc.

To prepare for large-scale simulations models with many pipes and devices for the Insheim and Kizildere II geothermal powerplants, which will be carried out in GeoSmart tasks T5.3 and T5.4, a powerful User Interface has been developed. Several sample calculations have been performed and presented, both for single pipe and pipe networks. The simulator software has also been validated by comparison to analytical results for two cases, with good agreement.

# 7. REFERENCES

1. A. Stefansson, I.M. Galeczka, GeoSmart deliverable report D4.1 "Modelling of silica scaling potential", May 2020
2. Multiphase technology – the best Norwegian invention since 1980, https://www.ife.no/en/ife/ife_news/2012/flerfaseteknologien-beste-norske-oppfinnelse-siden-1980
3. H2020 Smartrec, Grant Agreement EE-17-2016-2017-723838, https://www.smartrec.eu/
4. H2020 GeoCoat, Grant Agreement LCE-GA-2018-764086, https://www.geo-coat.eu/
5. H2020 GeoPro, Grant Agreement LC-CS3-RES-14-2019 -851816, https://www.geosmartproject.eu/
6. H2020 GeoDrill, Grant Agreement LC-SC3-RES-11-2018-815319, https://www.geodrillproject.eu/
7. Eurostars ProCase, Grant Agreement 115090
8. Norwegian Research Council – FORSTERK, Grant agreement 322724.
9. M. Asker, O.E. Turgut, M.T. Coban, "A review of non-iterative friction factor correlations for the calculation of pressure drop in pipes", Bitlis Eren Univ. J. Sci & Technology, 2014.
10. M. Zaupa, "Thermo-hydraulic models and analyses for design optimization of cooling circuits and components of SPIDER and MITICA experiments", PhD thesis, 2016.
11. P. Kjellgren, C. Kalavrytinos, H. Yu, C.B. Jenssen, T. Peng, GeoPro deliverable report D2.2 "Transient 1D FAS with existing thermodynamic models", April 2021.
12. Fabre, J., Line, A. Modeling of two-phase slug flow, Annu. Rev. Fluid Mech, 1992
13. PHREEQC Ver. 3; "A computer Program for Speciation, Batch-Reaction, One-Dimensional Transport, and Inverse Geochemical Calculations", https://wwwbrr.cr.usgs.gov/projects/GWC_coupled/phreeqc/
14. P. Kjellgren, H. Yu, C.B. Jenssen, T. Peng, Geo-Coat deliverable report D7.3 "Geothermal Flow Assurance Simulator", Nov. 2019
15. P. Kjellgren, C.B. Jenssen, H. Yu, T. Peng, GeoDrill deliverable report D7.1 "Geothermal Well Flow Assurance Simulator", Jan. 2021
16. NORSOK standard M-506, *CO2 corrosion rate calculation model,* Rev. 2 June 2005, Report, https://www.standard.no/

17. S. Nesic et al, *FREECORP™ 2.0 Theoretical Background and Verification,* Ohio University, 2018, https://www.icmt.ohio.edu/web/software/public/release/FREECORPTM.pdf
18. Recommended Practice RP O501, *Erosive wear in piping systems,* Revision 4.2 – 2007, Det Norske Veritas, http://www.dnv.com
19. O. Bratland, "Pipe Flow 1: Single-Phase Flow Assurance", 2009
20. H2020 WeldGalaxy, Grant Agreement 822106, https://www.weldgalaxy.eu/
21. P. Kjellgren, T. Peng, T. Mortensen, A. Lundbäck, WeldGalaxy Report D11.1, "Report on Welding Templates & Meta-Modelling, Iteration 2", Nov. 2020
22. H2020 GeoHex, Grant Agreement 851917, https://www.geohexproject.eu/
23. P. Kjellgren, J. Hyvärinen, "An Arbitrary Lagrangian-Eulerian finite element method", Computational Mechanics 21, 81–90 (1998). https://doi.org/10.1007/s004660050285
24. P. Kjellgren and L. Davidson. "**Large Eddy Simulation of Turbulence Flow Noise on Streamers**", SEG Annual Meeting, Houston, 25-30 Oct., 2009
25. P. Kjellgren, C.B. Jenssen, T. Peng, GeoDrill deliverable report D4.1 "Design and simulation of fluidic amplifier", Nov. 2019
26. F. Zhang, H. Begg, N. Kale, S. Irukuvarghula, V. Wittig, K. Mallin, B.A. Rodriguez, F. Chowdhury, M. A. Hoque, S.N. Karlsdottir, G.O. Boakye, P. Kjellgren, "Geo-Drill: Development of novel and cost-effective drilling technology for geothermal systems", WGC 2021
27. Andy Gibbs, Ben William Robinson, Sylvie Rougé, Hussam Jouhara, A K M Asaduzzaman, Mohammed Chowdhury, Per Kjellgren, Paolo Taddei Pardelli, Niccolò Ciuffi, "**Heat Recovery at High Temperature by Molten Salts for High Temperature Processing Industries**", AIP Conference Proceedings, 74th Annual Conference, Italian Thermal Engineering Association, 2019, https://aip.scitation.org/doi/pdf/10.1063/1.5138821
28. Taylor, G.I. (1954) The disperson of matter in turbulent flow through a pipe. Proceedings of the Royal Society, 223(1155):446-468
29. Hart J., Guymer I., Jones A., Stovin V. (2013) Longitudinal Dispersion Coefficients Within Turbulent and Transitional Pipe Flow. GeoPlanet: Earth and Planetary Sciences
30. Seo, Il Won, "Advanced Environmental Hydraulics", Lecture Notes, Seoul National University, 2010